ANKE Internal Report

Momentum correlation of particles recorded in the ANKE forward detector

S. Dymov, A. Kacharava, V. Komarov, S. Yaschenko

Jülich, October 2001

The absolute values (p_1 and p_2) of momentum of two particles in any three-particle final state process are strictly correlated (taking into account the two-solutions ambiguity), if the particles are emitted at fixed directions (θ_1,ϕ_1 and θ_2,ϕ_2). It is evident from the following. A three-particle process has 9 free kinematical parameters; the energy-momentum conservation results in 4 links, two directions are determined by 4 parameters. So a single parameter stays free. If to choose the absolute value of momentum of one of the particles, the entire kinematics is fixed, including the absolute value of the momentum of the second particle).

The correlation should conserve to some extent if the precise directions are changed by some restricted solid angles around the directions. The forward detector (FD) of ANKE accepts the secondaries with the polar angle of emission from zero up to about 16^0. However, this range of the angle is esentially reduced for particles of definite momentum (see Fig.1), and moreover, it is limited by 5^0 for particles with full 2π-radian azimuthal angle acceptance. Therefore, one may expect existence of significant kinematical correlation for particles recorded in the detector even without any additional kinematical cuts. Indeed, the simulations made in preparing the April'2000 beam-time (see the folder 'Experimental conditions at 0.5 GeV and 2.0 GeV') revealed such correlation. Among many different distributions we got distribution of events from the $pp \to pp\pi^0$ process at the plot: momentum of one particle versus momentum of the other. A prominent feature of this distribution consisted in concentration of the events along a rather narrow ($\Delta p \approx$ 30 MeV/c) belt at the plot (Fig.2). The belt become much narrower when the proton pairs hitting only one FD hodoscope element have been selected. Since the simulation was done with the phase space event generator, the observed correlation could be only of a kinematical nature.

Just the first experimental data obtained in April'2000 and processed with a momentum reconstruction of two particles revealed the two-particle momentum correlations.

In the following we give an overview of the distributions obtained with Hydrogen (Figs. 3,7) and Deuterium (Figs. 5,9,11,13,15,17,19) targets. It is seen that main processes with two fast forward emitted positively charged particles are clearly observable at the plot. In the hydrogen case they are: $pp \to pp\pi^0, pp \to p\pi^+ n$ and $pp \to d\pi^+$. Possition of the corresponding belts and spots are well reproduced by simulation (Figs. 4,6,8,10,12,14,16,18,20). All the distributions are symmetric relative the line $p_1 = p_2$ since the numbers (1) or (2) are assigned to the recorded particles in the pairs accidentally. The form of the three-particle belts evidentaly depends on masses of the particles in the pair.

The advantage of the data representation at the momentum-momentum plot consists in some points:

– Since no additional cuts (energy losses, TOF, etc.) are imposed all the processes with 2 positive particles hitting the detector are seen simultaneously, at the same plot. Therefore, the relative intensity, possible 'overlapping', background conditions for the processes are clearly visible.

– Dynamics of change of the intensity and relative position of the plot with change of the beam energy is well obsevable.

– A proper choice of the momentum area for selection of a process under consideration may be easly done.

– Immediate comparison of the reactions at different targets can be done. In the hydrogen-deuterium case one sees at once that the processes taking place on the hydrogen target reveal itself clearly on the deuterium in a quasifree model. Some new processes ($pd \to ppn, pd \to ^3 H\pi^+$) certainly arise with the deuterium.

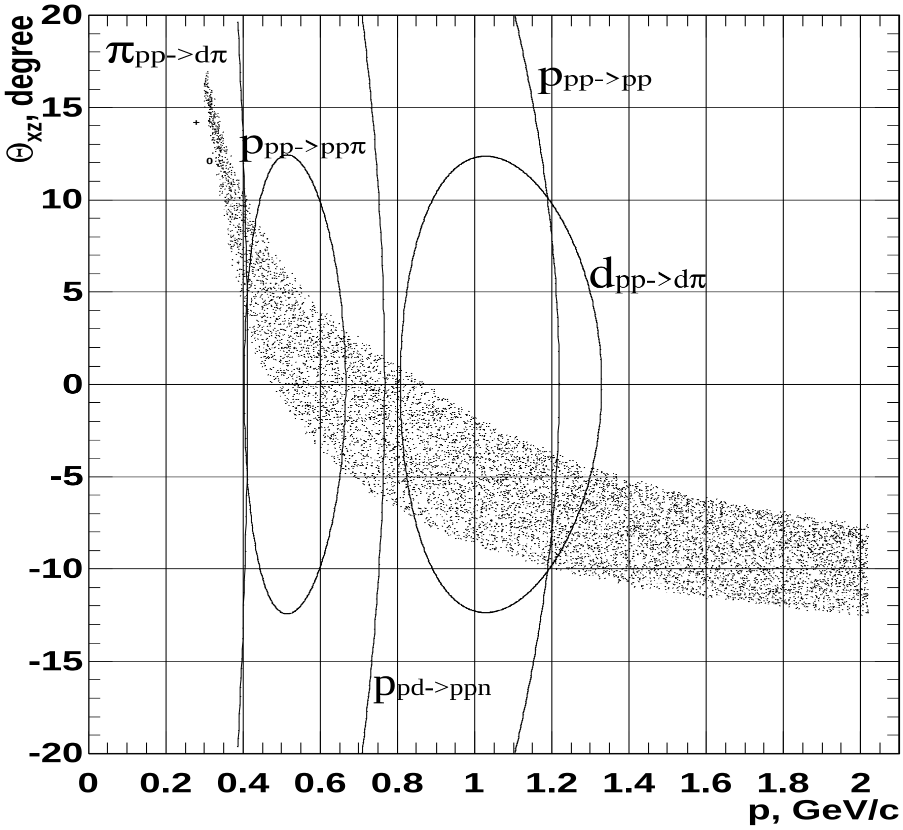

Fig. 1. FD angular-momentum acceptance

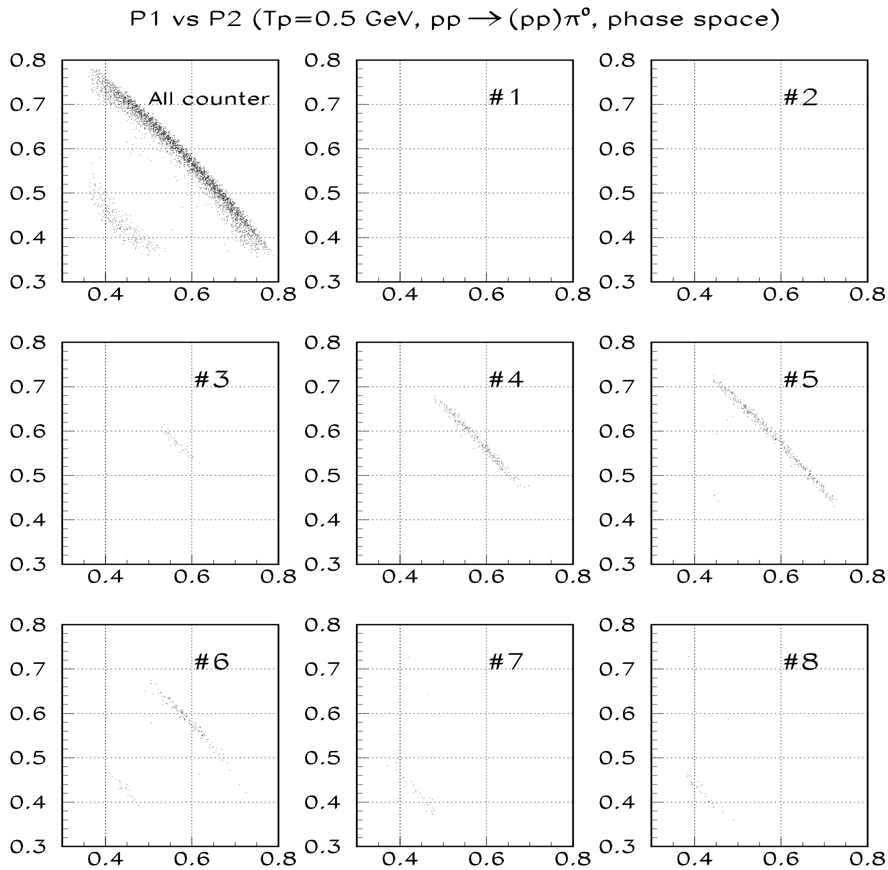

Fig. 2. Simulated data

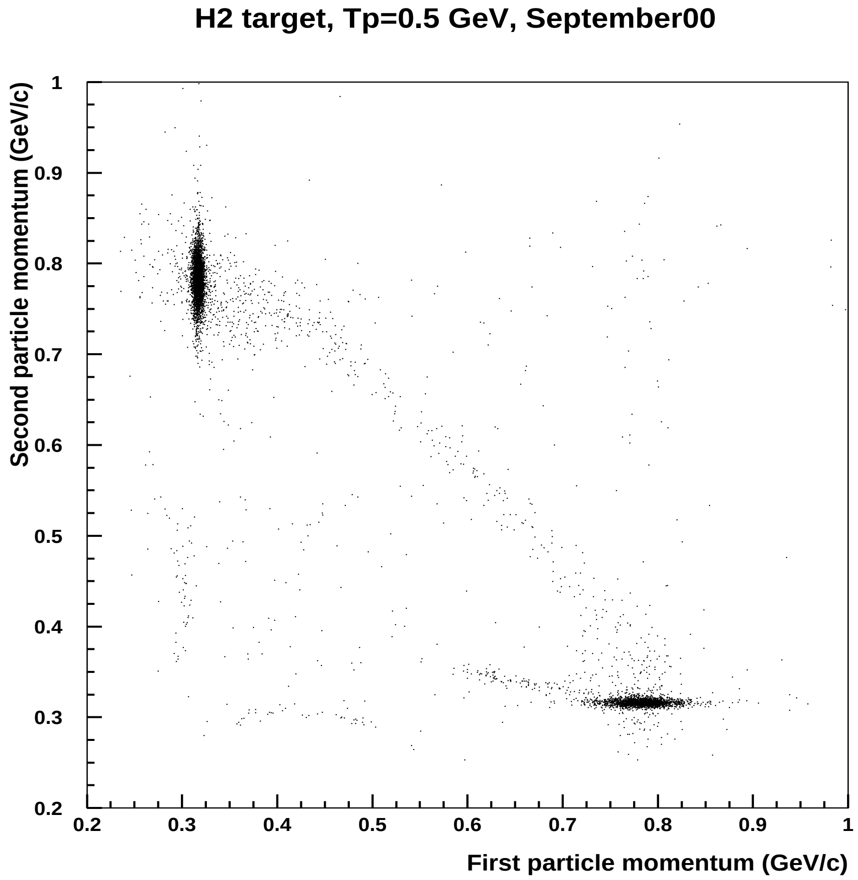

Fig. 3. Experimental data

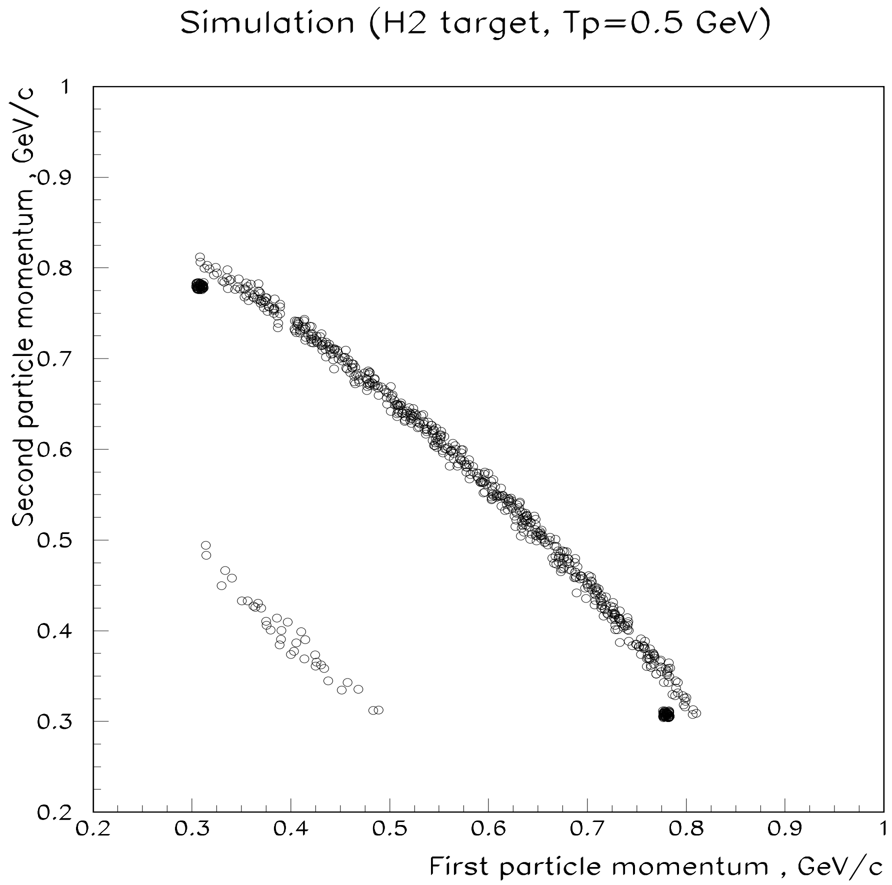

Fig. 4. Simulated data (Run conditions Sep.00)

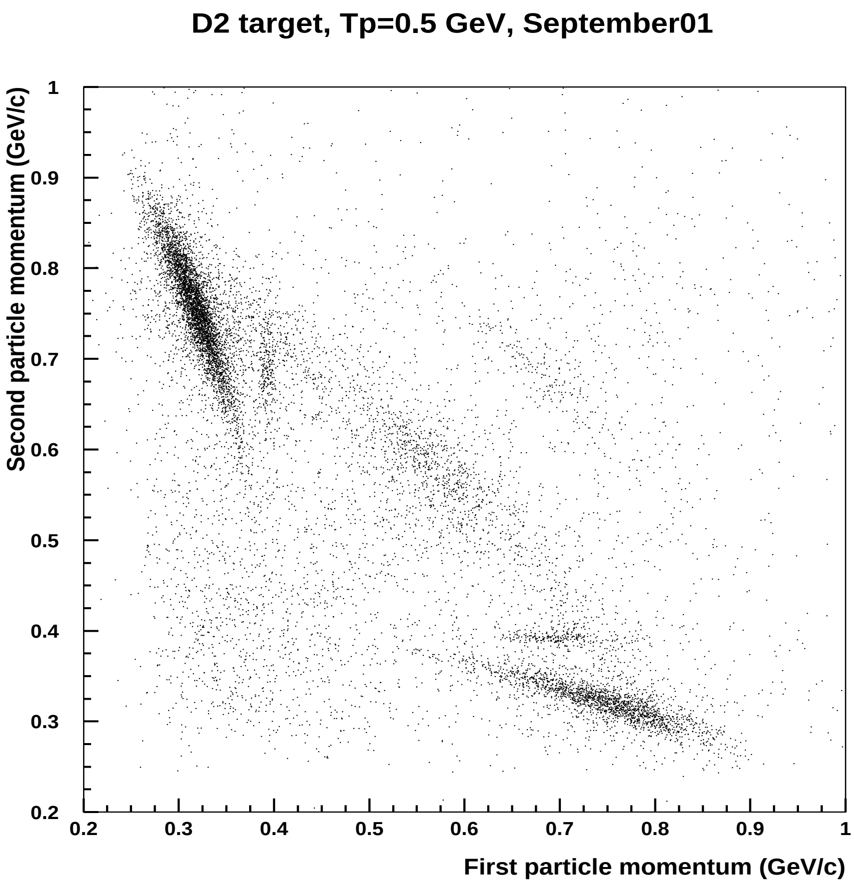

Fig. 5. Experimental data

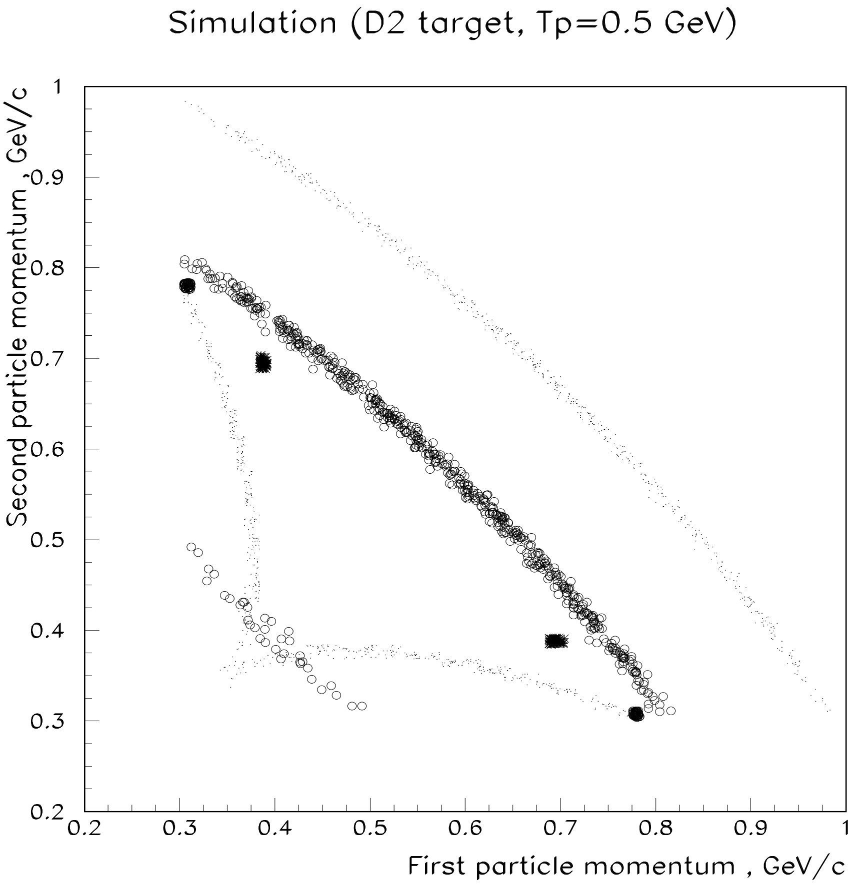

Fig. 6. Simulated data (Run conditions Sep.01)

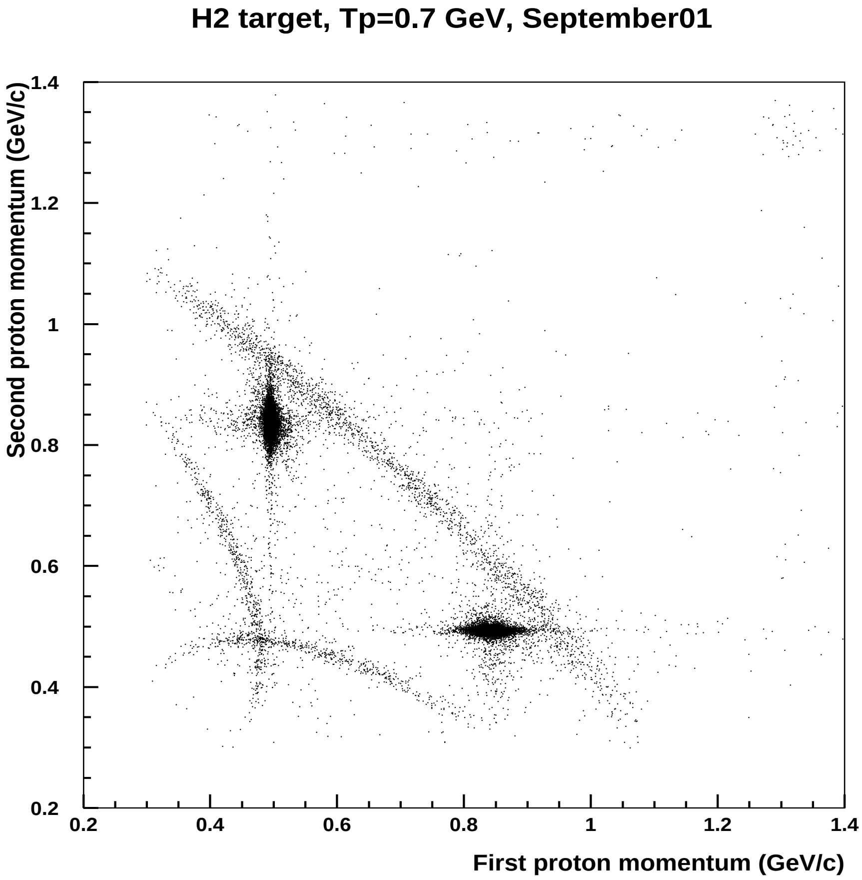

Fig. 7. Experimental data

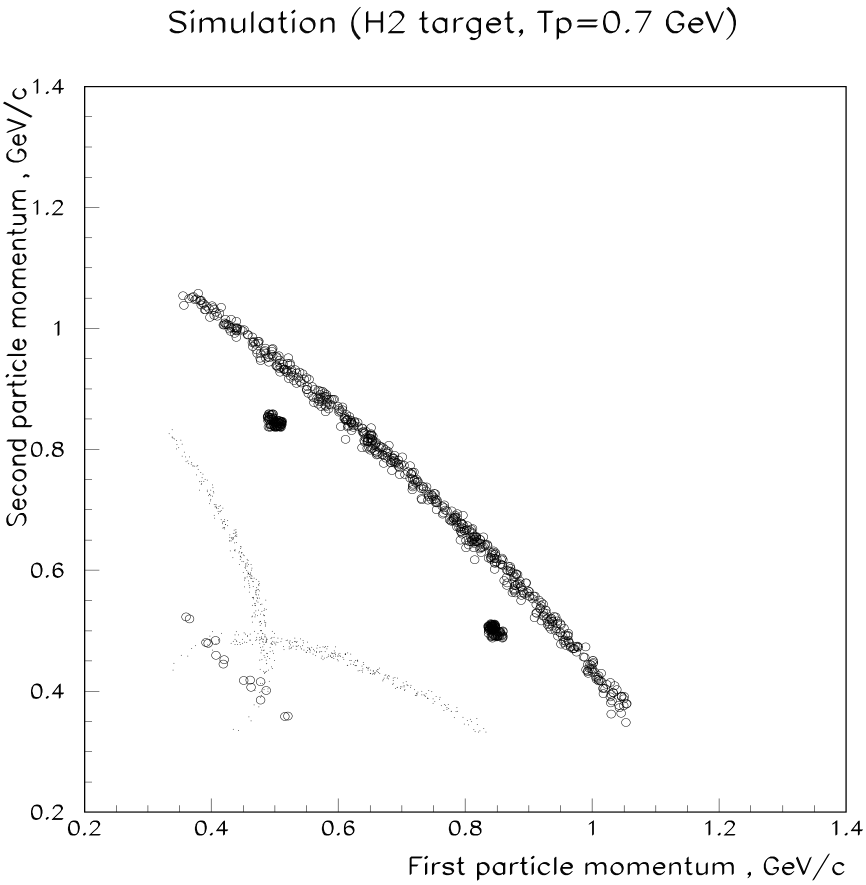

Fig. 8. Simulated data (Run conditions Sep.01)

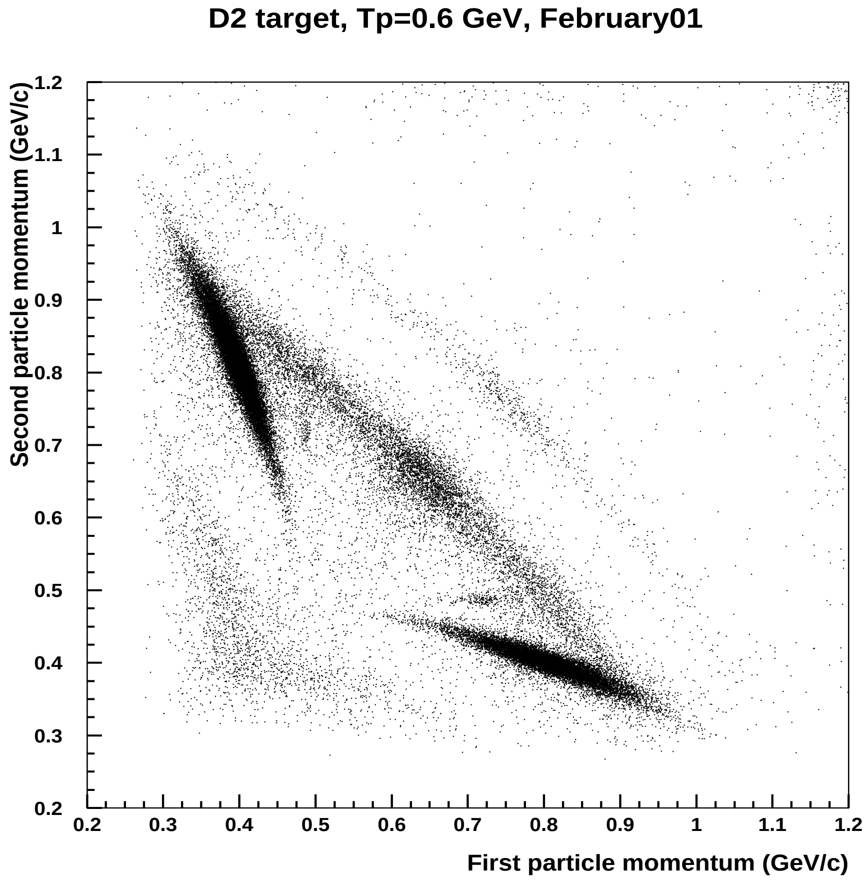

Fig. 9. Experimental data

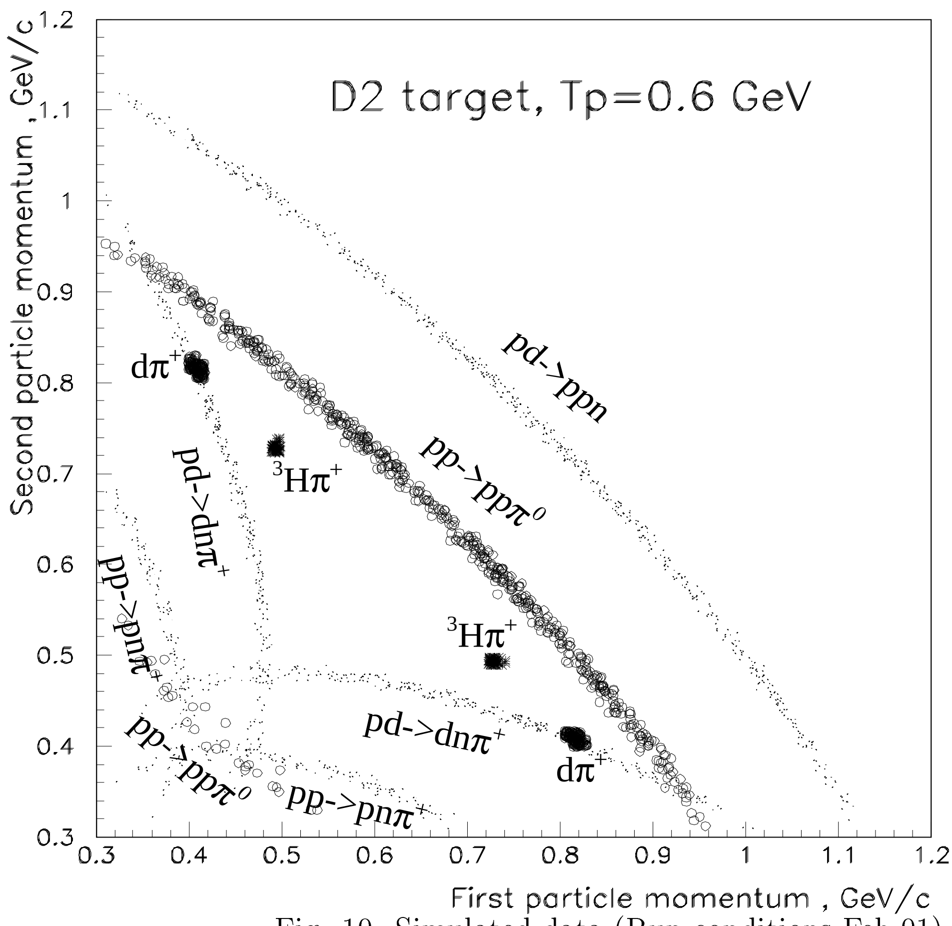

Fig. 10. Simulated data (Run conditions Feb.01)

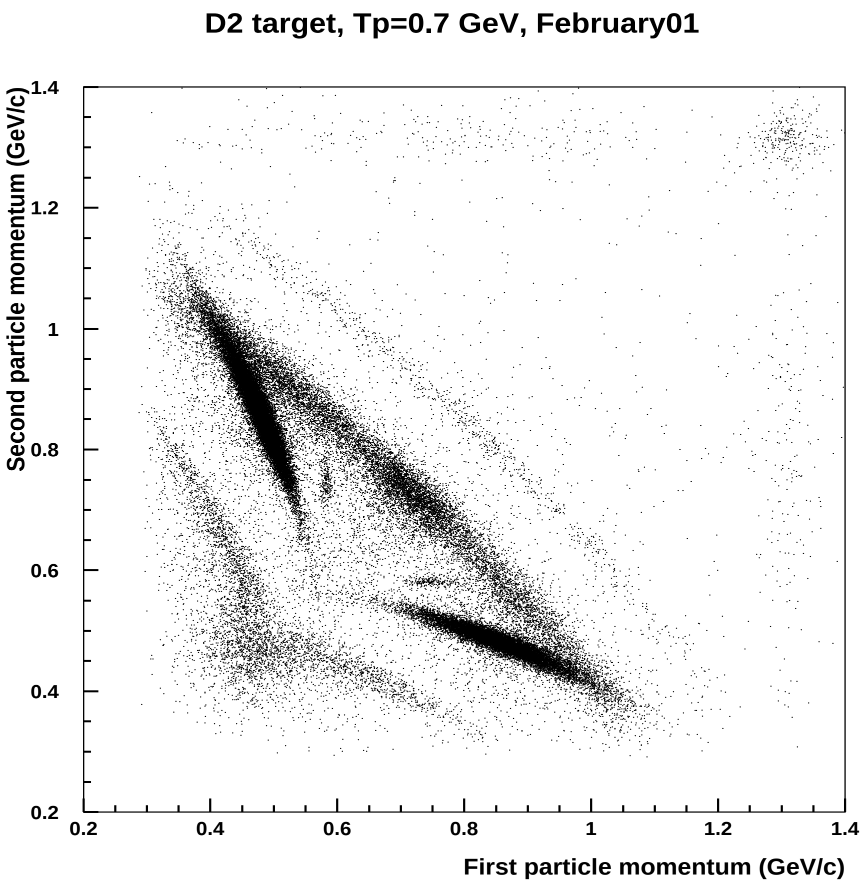

Fig. 11. Experimental data

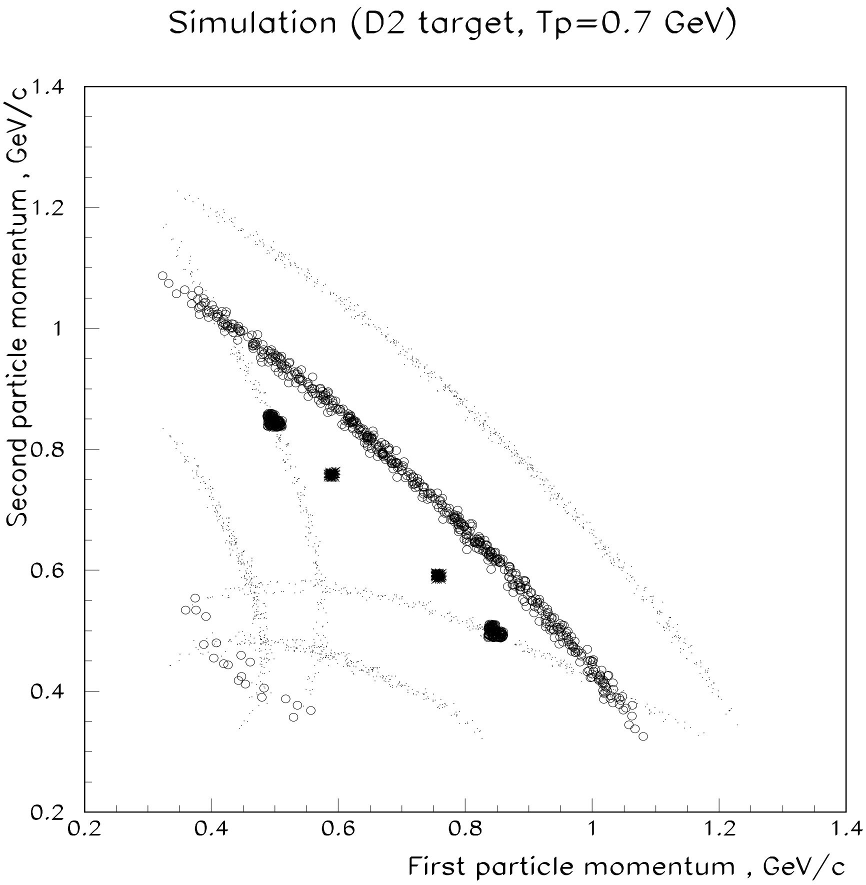

Fig. 12. Simulated data (Run conditions Feb.01)

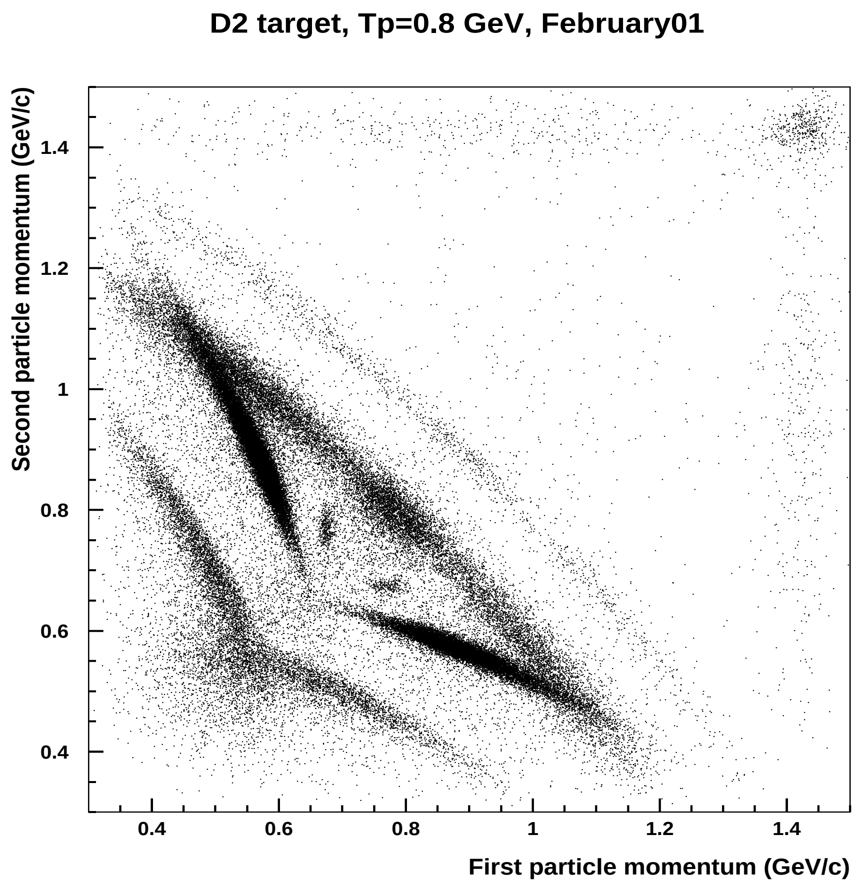

Fig. 13. Experimental data

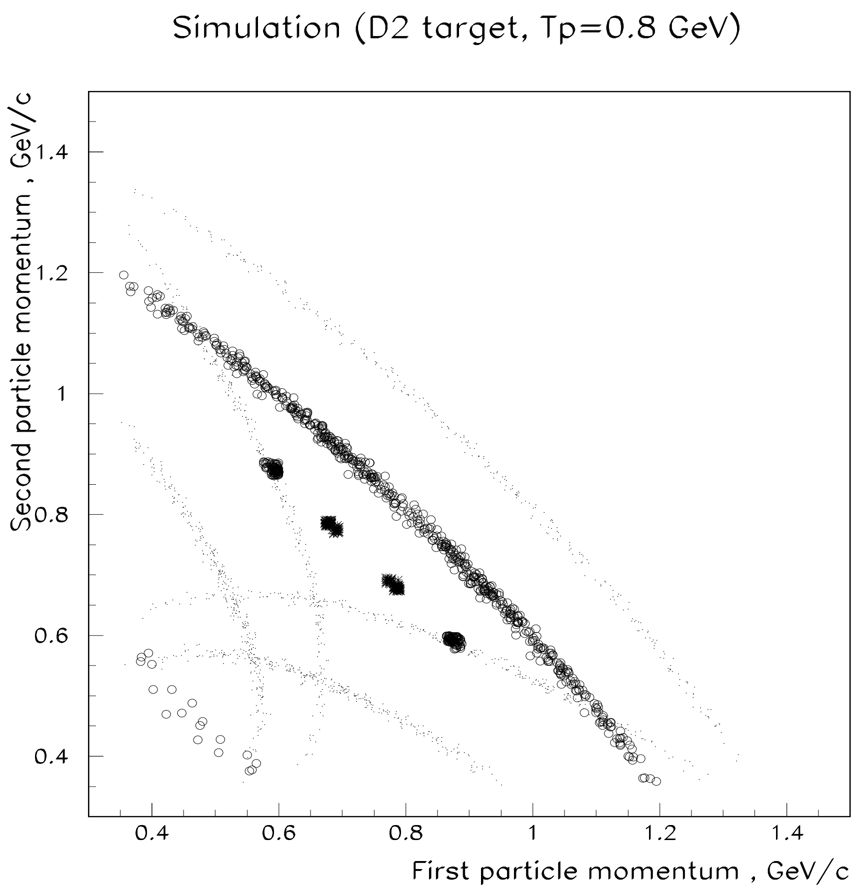

Fig. 14. Simulated data (Run conditions Feb.01)

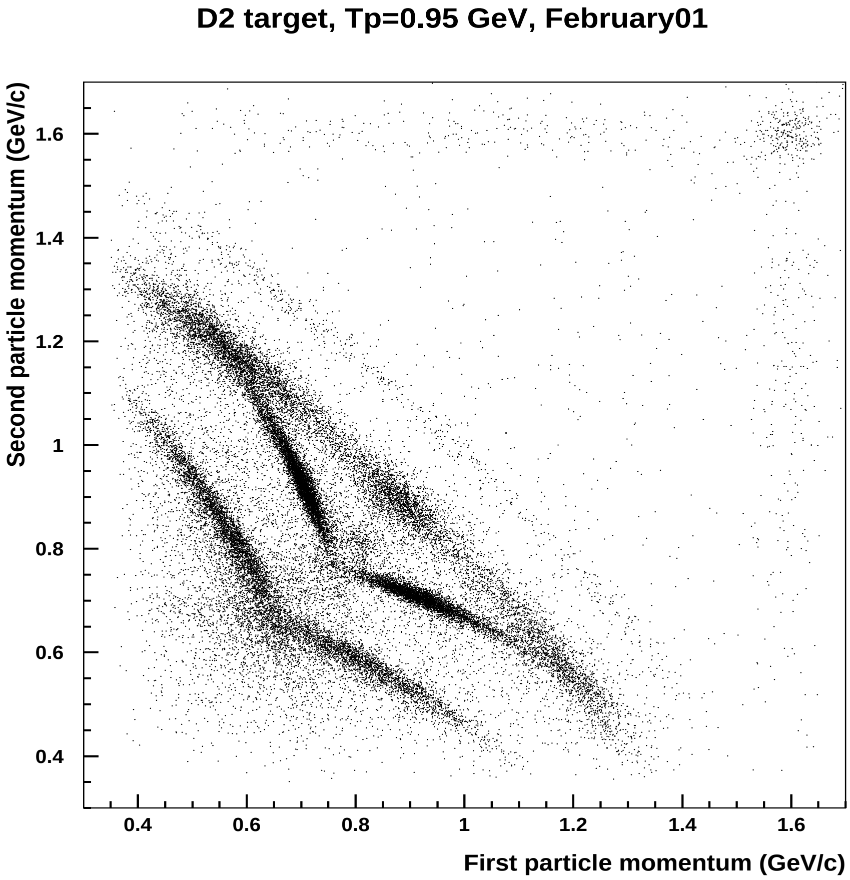

Fig. 15. Experimental data

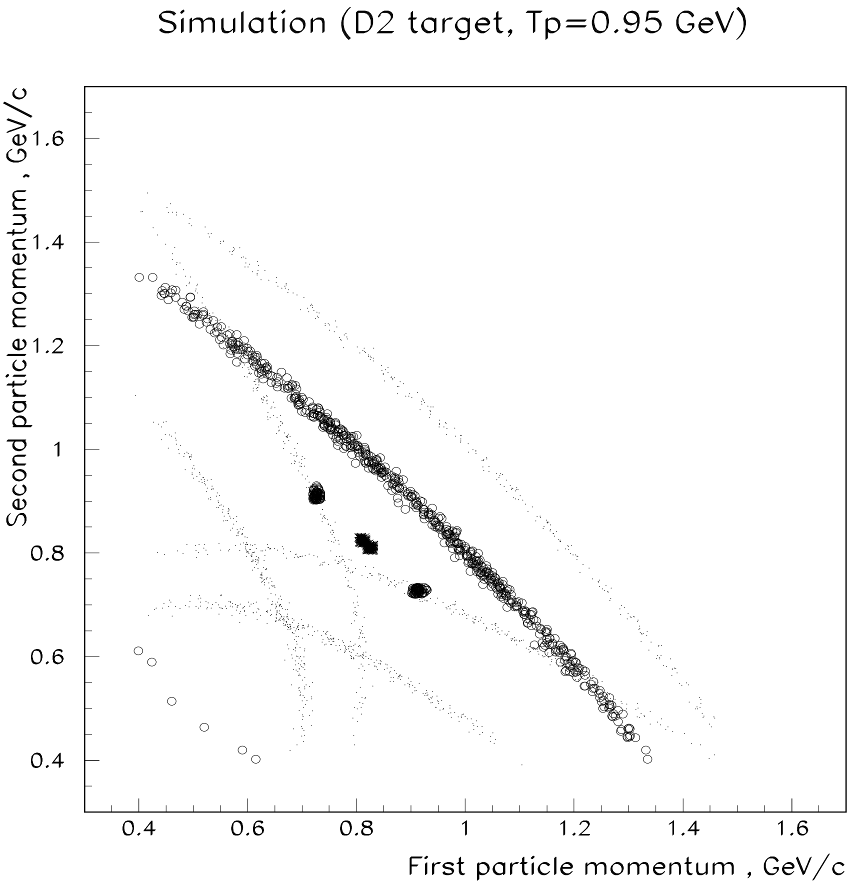

Fig. 16. Simulated data (Run conditions Feb.01)

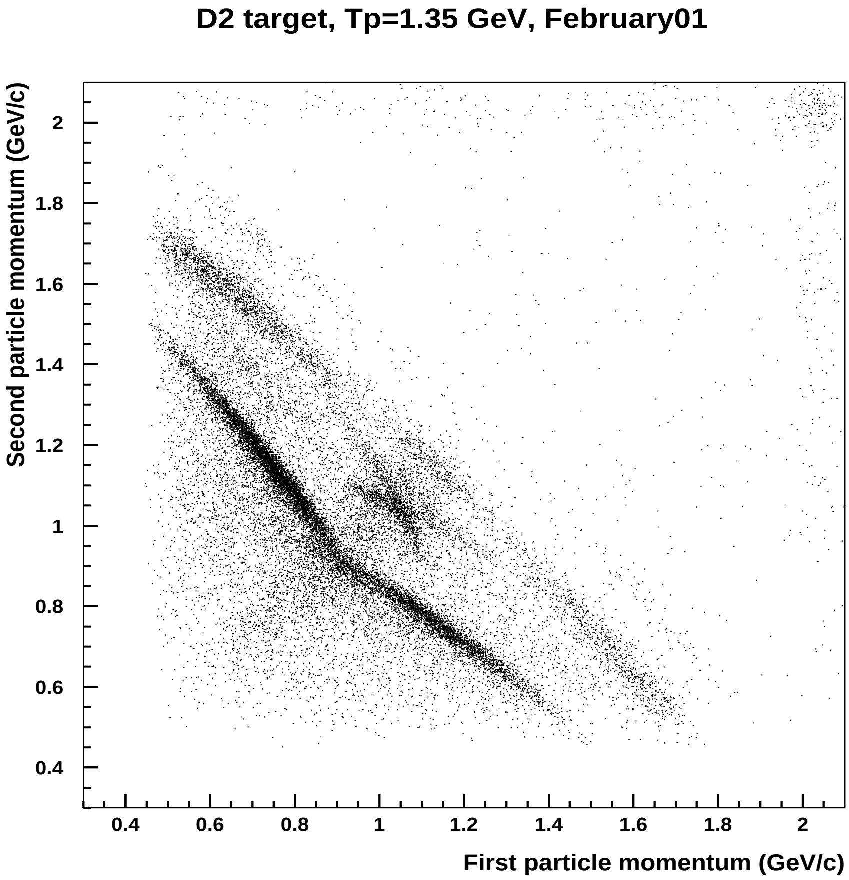

Fig. 17. Experimental data

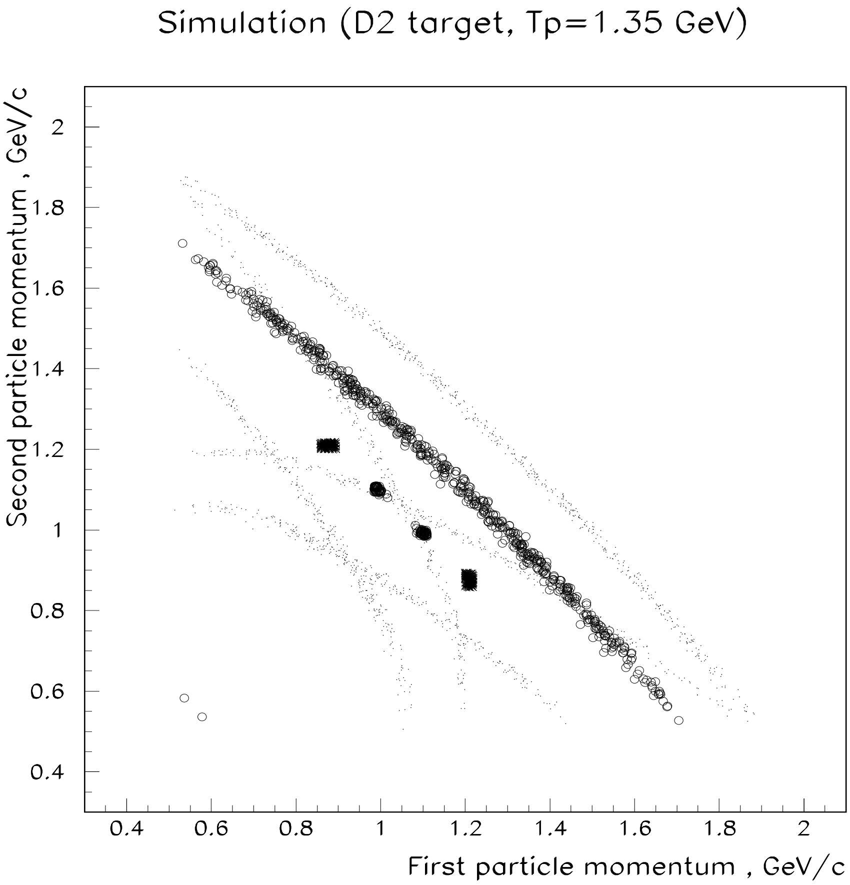

Fig. 18. Simulated data (Run conditions Feb.01)

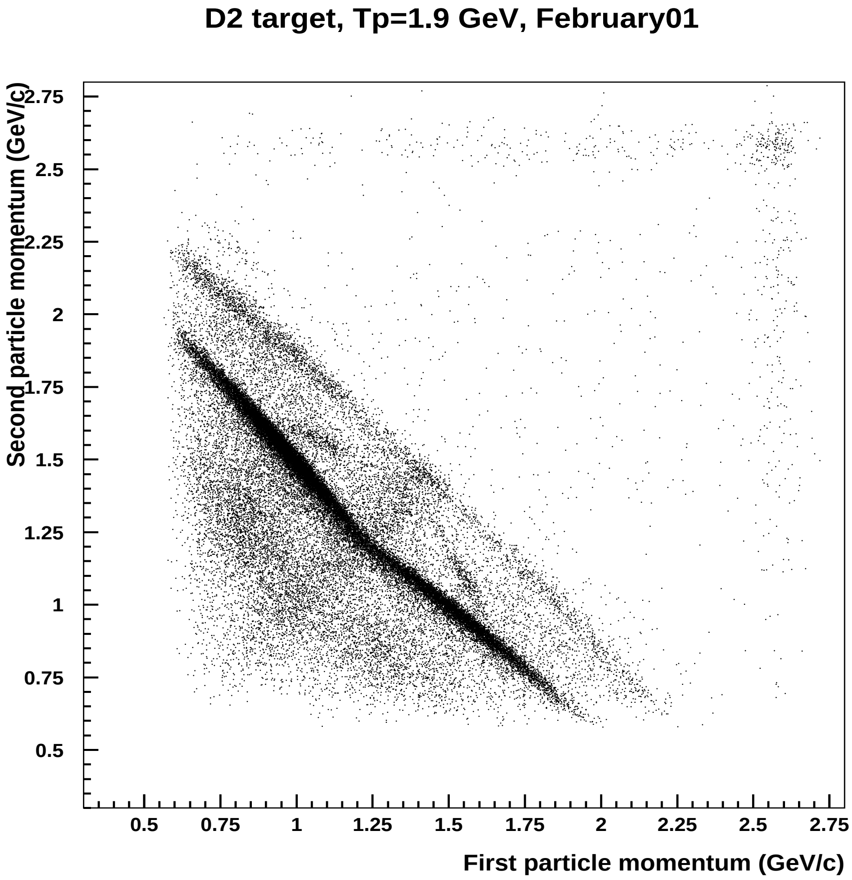

Fig. 19. Experimental data

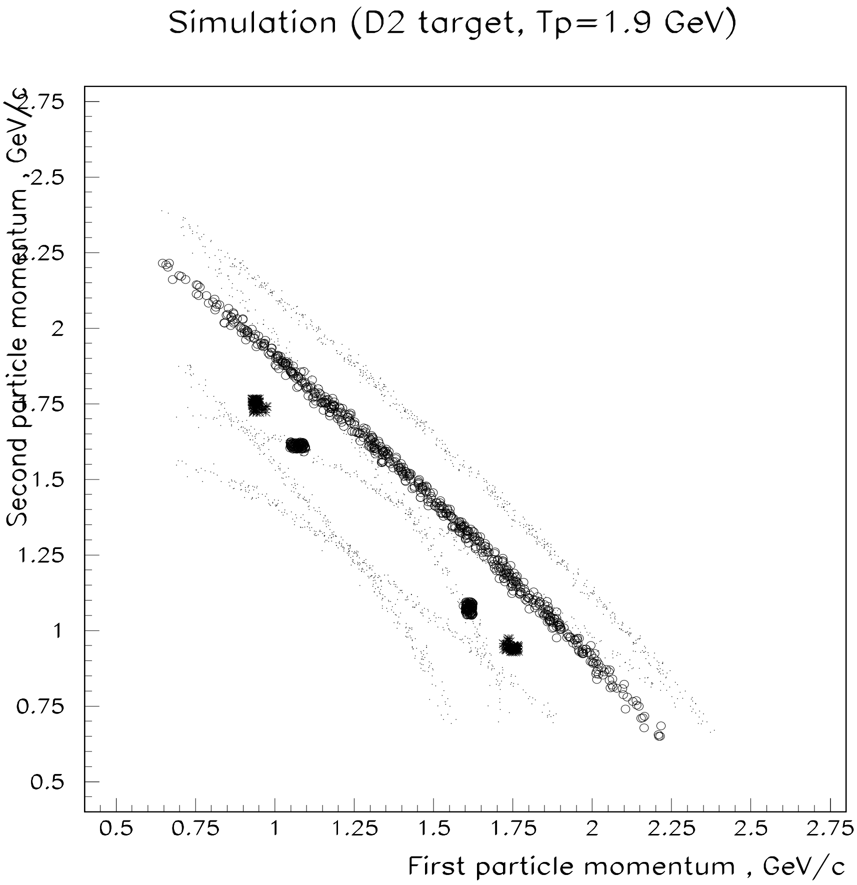

Fig. 20. Simulated data (Run conditions Feb.01)